Desalination and Water Treatment
www.deswater.com
doi: 10.5004/dwt.2020.26403

208 (2020) 273–286
December

Hydrogen evolution via water splitting using TiO_2 nanoparticles immobilized on aluminosilicate mineral: synergistic effect of porous mineral and TiO_2 content

Rojiar Akbari Sene[a,*], G.R. Moradi[b], S. Sharifnia[b], Farhad Rahmani[a]

[a]*Department of Chemical Engineering, Faculty of Engineering, University of Kurdistan, Sanandaj, Iran, Tel. +98 87 33660073; Fax: +98 87 33668513; emails: r.akbari@uok.ac.ir (Rojiar Akbari Sene), F.rahmanichiyane@uok.ac.ir (Farhad Rahmani)*
[b]*Chemical Engineering Department, Catalyst Research Center, Razi University, Kermanshah, Iran, emails: gmoradi@razi.ac.ir (G.R. Moradi), sharif@razi.ac.ir (S. Sharifnia)*

Received 15 December 2019; Accepted 23 July 2020

ABSTRACT

Hydrogen evolution via water splitting was investigated over the nanostructured TiO_2/clinoptilolite photocatalyst with the aim of exploring the natural zeolitic support potential and assessing the effect of TiO_2 content on the photocomposite reactivity. To this aim, a series of clinoptilolite supported TiO_2 photocatalysts varying in titania content (10, 30, and 50 wt.%) were synthesized by facile solid-state dispersion method. The characterization results indicated that clinoptilolite utilization could not only reduce the recombination of electron–hole pairs but also promote the distribution of metallic particles and decrease the TiO_2 particle agglomerations. These features were more prominent as 10 wt.% of TiO_2 was loaded. Accordingly, supporting TiO_2 over natural zeolite helped to boost the hydrogen evolution. The highest photocatalytic activity, 282.48 μmol/g TiO_2 h, was obtained for the TiO_2(10%)/natural zeolite sample which was about four times more than that of bare TiO_2. However, the excessive loading of TiO_2 severely covered the surface of natural zeolite, afforded the aggregations of metallic particles and thereupon, weakened the contact between clinoptilolite and TiO_2 and also, the separation efficiency of electron–hole pairs, resulted in the H_2 production loss.

Keywords: Hydrogen production; Water splitting; Photocatalysis; TiO_2 nanocomposites; Clinoptilolite support

1. Introduction

Massive global utilization of fossil fuels has intensified worldwide attend to global warming and reduction of natural energy resources. Because of current energy and environmental problems, the identification of appropriate alternative and renewable energy sources such as hydrogen is so important [1–3]. Hydrogen is considered as an excellent green fuel for the future since it has a high specific energy density, zero-emission of greenhouse gas, and is easily storable [4,5]. Currently, the majority of hydrogen demands obtain from steam reforming of natural gas and petroleum, which also produces large CO_2 gas [6].

In recent years, many investigations have been done to develop other approaches to produce hydrogen from renewable resources [7]. Photocatalytic water splitting over semiconductors is one of the ideal ways to produce H_2 from clean and renewable sources [2,8]. This reaction initiates by the absorption of a photon with energy equal to or higher than the band gap of the semiconductor. This generates excited photoelectrons in the conduction band (CB) and holes in the valence band (VB) of the photocatalyst. Then, water molecules are reduced and oxidized by excited electrons/holes and produce hydrogen and oxygen, respectively [9,10]. In many presently known semiconductors, titanium dioxide (TiO_2) has been regarded as

* Corresponding author.

a good candidate for photocatalytic hydrogen generation due to its chemical stability, photocorrosion resistibility, environmental friendly, and its low cost and abundance [11–13]. However, when TiO_2 is utilized in hydrogen production via water splitting, some important problems arise. The fast bulk recombination of electron–hole pairs, the low surface area of the photocatalyst and low recovery efficiency of fine TiO_2 particles are considered as critical points that constrain the practical application of titania for large-scale hydrogen production [14,15].

To overcome the shortcomings aforementioned, one of the effective strategies is the immobilization of TiO_2 particles on highly porous support. The combination of porous materials and TiO_2 semiconductor may provide several advantages for photocatalytic reactions including: (i) decreasing electron–hole recombination as a determining factor in photocatalytic reactions; (ii) the improvement of light absorption due to trapping in the porous structure; (iii) the formation of ultrafine TiO_2 particles on easily-separable micro-sized support; and (iv) a superior surface area and a higher surface density of active sites for photocatalytic reactions [16,17]. The deposition of TiO_2 on various supports such as silica [18,19], activated carbon [20–22], clay and zeolites [23–26], has been proved to be an efficient route to enhance photocatalytic performance.

Among various supports, aluminosilicates are considered as a one of the most promised photocatalyst support [16,27,28], due to their specific properties such as high surface area, unique structures, uniform pores and channels, easily tunable chemical properties, high thermal stability, and excellent absorption capacity [17,29,30]. The framework of zeolite is known to improve the photocatalytic activity of the entrapped TiO_2 by prolonging the separation of the photogenerated electrons and holes [31]. In addition, depending on the adsorption sites, zeolites behave as electron donors and acceptors toward the guest species [23]. Hence, semiconductor-incorporated zeolites have recently gained importance in photocatalytic reactions [28,32]. However, due to complex and time-consuming synthesis and the high cost of synthetic zeolites, the practical application of these supports is limited. Natural zeolites are cheaper and abundant storage as compared with synthetic zeolites. Considering the low cost, abundance, easily available, and high chemical stability, clinoptilolite seems to be efficient support applicable for photocatalytic hydrogen production [33–35]. In this context, Akbari Sene et al. [36] introduced sonochemically synthesized TiO_2/clinoptilolite nanocomposite as a new efficient photocatalyst in the water-splitting process for hydrogen production. They sonochemically dispersed TiO_2 nanoparticles over clinoptilolite and discussed over the effect of ultrasound irradiation on the photocatalytic properties and performance. In another work, they modified clinoptilolite support by various chemical treatment methods and used in the synthesis of sonochemically prepared TiO_2-based photocatalysts [37]. Although some studies in association with employing clinoptilolite-supported TiO_2 photocatalyst in water splitting process are done, the evaluation of the synergistic effect of clinoptilolite and TiO_2 content was not found in the literature.

Therefore, the current research is emphasized on studying the effect of clinoptilolite usage as a low-cost and availability support, the amount of TiO_2 loading and further discovers the potential of clinoptilolite supported TiO_2 photocatalyst in the hydrogen production. In fact, the main goal of this work is the development of low-cost and practical TiO_2-based photocatalyst using low-cost and availability materials, facile, and cost-effective deposition method, and optimum TiO_2 loading. To this aim, various TiO_2-clinoptilolite composites with different titania contents ranged from 10 to 50 wt.% were prepared via the solid-state dispersion (SSD) method. The effect of clinoptilolite and TiO_2 content on microstructure and property of the as-prepared photocatalysts was characterized by X-ray diffraction (XRD), field emission scanning electron microscopy (FESEM), energy-dispersive X-ray spectroscopy (EDX), Brunauer–Emmett–Teller (BET), Fourier-transform infrared (FTIR), photoluminescence (PL), and ultraviolet-visible (UV-vis) absorption. The activity of synthesized photocatalysts for hydrogen evolution from water containing methanol as a sacrificial agent was investigated under UV excitation. As a comparison, bare TiO_2 and clinoptilolite were also prepared and employed.

2. Materials and methods

2.1. Materials

The semiconductor employed in the synthesis of TiO_2/natural zeolite photocomposites was commercial TiO_2 (Degussa P-25 having 80% anatase and 20% rutile, the surface area of 50 m^2/g, and the mean particle size of 25 nm). The natural clinoptilolite tuffs used in this study as the photocatalyst supports were taken from the Mianeh deposit, located in the East Azerbaijan region of Iran. The analytical grade of ethanol (Merck, Germany) and methanol (Merck, Germany) as a dispersing agent and sacrificial agent, respectively, were used. All of the materials were used as received without any further purification. Double distilled water was used in the preparation of all photocatalysts and also, the photocatalytic H_2 production tests.

2.2. Preparation of photocatalysts

TiO_2-natural aluminosilicate photocatalysts were synthesized by a facile and cost-effective approach known as solid-state dispersion (SSD) method. Initially, TiO_2 (P-25 Degussa) was mixed thoroughly with aluminosilicate using ethanol as a dispersing agent in agate pestle and mortar, the dispersing agent was then evaporated during blending. After drying at 110°C overnight, the prepared samples were calcined in air at 500°C for 6 h to obtain TiO_2-natural zeolite photocatalysts. The resulting TiO_2/natural zeolite composites depending on the amount of TiO_2 loading were denoted as $TiO_2(x)$/NZ. The term "x" represents the nominal weight percentage of TiO_2 in the composite (x: 10, 30, and 50). For preparing the aluminosilicate support, at first, the crushed clinoptilolite tuff was screened to achieve a particulate size distribution in the size range of approximately 44–53 μm. Then, the obtained powder was washed to eliminate the water-soluble and undesirable materials, and dried at 110°C for 24 h before its employment in the photocatalyst synthesis. The preparation details of the aluminosilicate and photocatalytic nanocomposites have been illustrated in Fig. 1.

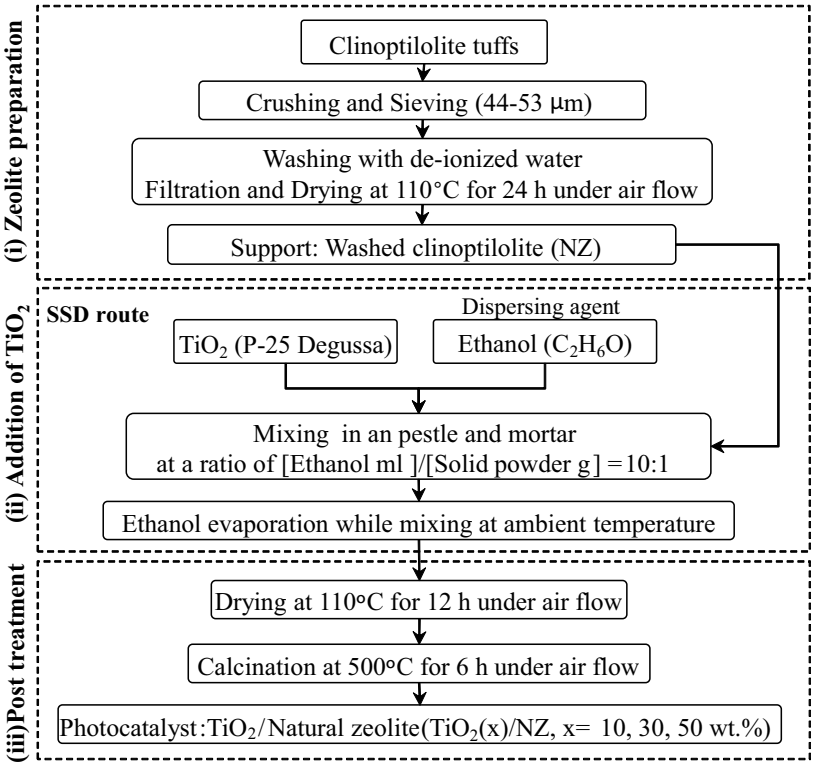

Fig. 1. Synthesis steps of photocatalysts.

2.3. Photocatalysts characterization

The crystalline phase and structure identification of samples were made by XRD analysis. The XRD patterns were recorded on a D-5000 diffractometer (Siemens, Germany) with Cu-Kα radiation coupled to an X-ray tube that works at a voltage of 30 kV and an emission current of 40 mA. Each sample was scanned in the angular region of 2θ = 2°–90° with a rate of 4°/min. The surface morphology of the prepared samples was examined by FESEM analyzer (VEGA\\-TESCAN, Czech Republic) equipped with a BSE detector for elemental analysis. Titanium surface densities (number of TiO_2 species per nm^2) were calculated by considering the Ti content measured by EDX and the S_{BET} and assuming all TiO_2 is exposed to the surface. The surface titanium density (Ti surface density, TiO_2 nm^{-2}) was calculated according to the following equation as:

$$\text{Ti surface density} = \frac{N_A \times x_{Ti}}{Mw_{Ti} \times S_{BET}} \times 10^{-18} \quad (1)$$

where N_A is Avogadro constant, x_{Ti} mass fraction of titanium in TiO_2/CLT (wt.%), Mw_{Ti} is the molecular weight of titanium (47.867 g mol^{-1}), and S_{BET} is the specific surface area of the catalyst (m^2 g^{-1}). The specific surface area of the prepared photocatalysts was calculated from the N_2 adsorption result using a Quantachrome (Model ChemBET3000, USA) instrument according to the BET equation. To identify surface functional groups, infrared spectra of KBr powder-pressed pellets were recorded at room temperature in the wavenumber range of 400–4,000 cm^{-1} on a UNICAM 4600 FTIR spectrophotometer. Diffuse reflection UV-vis spectra of the samples (UV-visible DRS) were recorded using a Jasco (model V-670) spectrophotometer equipped with an integrating sphere attachment using $BaSO_4$ powder as an internal reference. UV-vis spectra were carried out in the diffuse reflectance mode (*R*) and transformed to absorption intensity by using the Kubelka–Munk method. The PL spectra for photocatalysts were determined with a VARIAN CARY ECLIPSE fluorescence spectrophotometer in which a xenon lamp was employed as the excitation source with an excitation wavelength of 280 nm.

2.4. Photocatalytic test

Fig. 2 illustrates the apparatus used for photocatalytic reaction tests of the prepared samples. The photocatalytic production of hydrogen was carried out in an outer irradiation-type quartz reactor, which irradiated using three 125 W medium pressure mercury lamps. To maintain the system temperature at ca. 25°C, the photoreactor was equipped with a water-cooled condenser. In a typical run, 200 mg of the photocatalytic nanocomposite was suspended in 0.2 L aqueous solution containing 10% (v/v) CH_3OH as a sacrificial agent by a magnetic stirrer during the 4 h irradiation. Prior to the light on, the suspension inside the sealed photoreactor was purged with helium for approximately 0.5 h to discharge the dissolved air completely. The amount of hydrogen evolution was measured using a GC equipped with a TCD and Molecular Sieve 5 Å column. Finally, the photocatalytic activity was calculated and reported in the unit of μmol/g TiO_2 h.

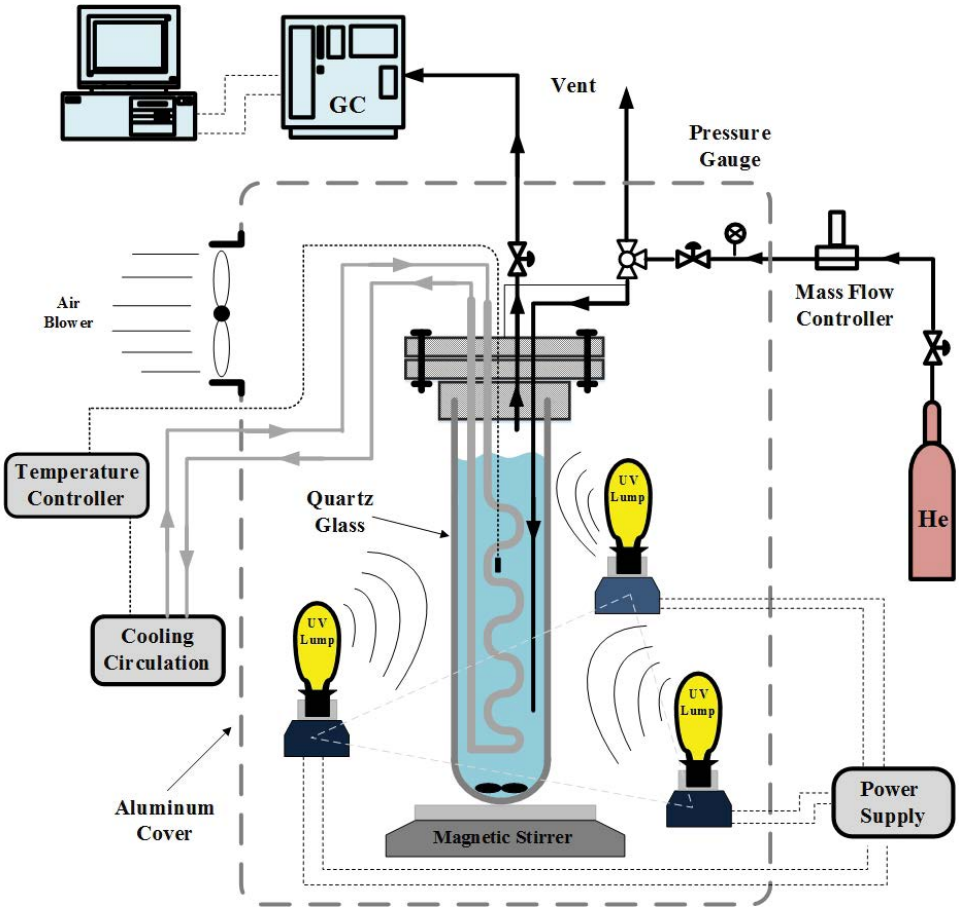

Fig. 2. Experimental setup for testing of the photocatalytic performance of synthesized photocatalysts used in water-splitting reaction.

3. Results and discussions

3.1. Photocatalyst characterization

3.1.1. XRD analysis

The recorded XRD patterns of the TiO_2/natural zeolite photocatalysts varying in TiO_2 content at 2θ = 5°–90° have been depicted in Fig. 3. A glancing over the XRD patterns reveals that the diffraction patterns corresponding to those of TiO_2 and clinoptilolite are observed over all the synthesized TiO_2/NZ photocatalysts. The illustrated peaks at 2θ = 9.8°, 11.2°, 22.4°, 22.7°, 26.1°, 28.2°, 30.0°, and 32.0° are attributed to clinoptilolite (JCPDS 00–025–1349) in the monoclinic phase [38–40]. As can be seen, the anatase and rutile phases of TiO_2 coexist in the structure of TiO_2-based samples. However, the rutile phase of TiO_2 is barely detectable in TiO_2 coated zeolite samples. The observable peak centered at 2θ = 27.1°, 35.5°, 40.6°, and 53.5°, is assigned to the rutile phase [41,42]. However, these peaks are not prominent in the XRD pattern of TiO_2(10%)/NZ sample and the major illustrated peaks at about 2θ = 25.2°, 37.9°, 48.3°, 53.8°, 55.3°, and 62.7° confirmed the existence of the anatase phase of TiO_2 [29,43]. Regarding the XRD pattern of bare natural zeolite, it can be identified that by gradually increasing TiO_2 content over clinoptilolite structure, the peaks related to the crystalline phase of TiO_2 appear and become intense obviously. In contrast, the intensity of clinoptilolite peaks in the synthesized samples diminishes. This decrease can be attributed to a dilution effect of the zeolite matrix in the photocatalyst and might be a sign of surface coverage of zeolite by TiO_2 nanoparticles as a result of its addition. No considerable decrease in the intensity of clinoptilolite diffraction peaks was observed by loading of 10 wt.% TiO_2. Accordingly, it seems that the severe surface coverage of zeolite occurred in the TiO_2 rich composites which are going to be supported by the FESEM and EDX analyses.

3.1.2. FESEM analysis

Fig. 4 shows the FESEM images of the synthesized composites with different TiO_2 loadings. As can be seen, the bare clinoptilolite sample has a blade-shaped structure, in agreement with that of clinoptilolite reported in the literature [38]. By loading of TiO_2, spherical particles are formed either as nanoparticles or clusters attached to the zeolite matrix of clinoptilolite. It is obvious that all the synthesized TiO_2-based photocatalysts have nanometric surface particles. Nanoparticles provide more reactive sites and result in high photocatalytic performance of the TiO_2-based composites. The micrometer-sized of the supported TiO_2 nano-particles is also noteworthy which facilitates the

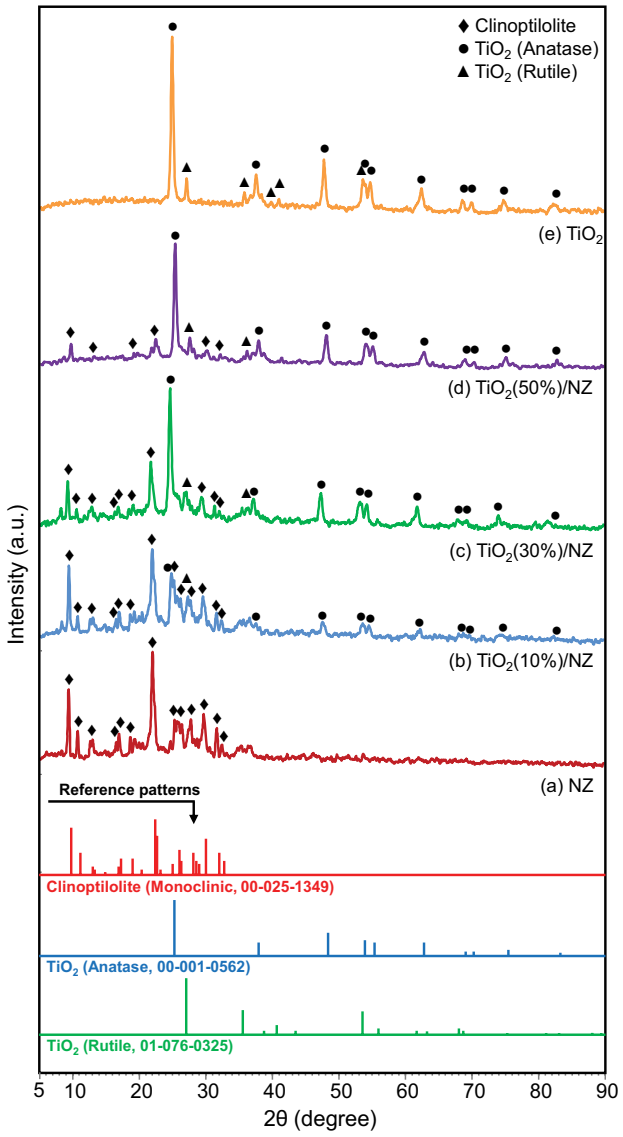

Fig. 3. XRD patterns of synthesized photocatalysts: (a) NZ, (b) TiO_2(10%)/NZ, (c) TiO_2(30%)/NZ, (d) TiO_2(50%)/NZ, and (e) TiO_2.

separation process, improving the reusability of the samples. A close examination of the FESEM results also revealed that no obvious conglutinated particles were observed at low TiO_2 loading (10 wt.%), confirming the finely dispersed TiO_2 nanoparticles. In this case, the size distribution of TiO_2 particles was found to be narrower than that of pristine TiO_2. Increasing TiO_2 loading would result in higher numbers of active sites for the photocatalytic process. However, by further increasing TiO_2 loading, the zeolite particles are covered with TiO_2 clusters insofar as the presence of zeolite micro-particles is hardly distinguished. In addition, some agglomerations appear. The particle agglomeration and much blocking of support's pores as the disadvantageous side effects of excessive loading of TiO_2 may lead to worse photocatalytic performance. It seems that these problems can be minimized by loading of 10 wt.% TiO_2.

3.1.3. EDX analysis

Fig. 5 demonstrates the EDX micrographs of the as-prepared samples. Based on the EDX spectra, all chemicals employed in the preparation of all nanostructure composites are detected. Within the detection limit of the apparatus, any impurities in the sample structure are not also observed. Besides, the titanium element content of samples measured by the EDX analysis is close to its nominal content. These observations, together with the attainment of the needed crystalline phases are evidence for the successful preparation. The comparison of the Ti dot-mappings indicates that loading of 10 wt.% TiO_2 provokes a better dispersion which is going to affect the photocatalytic activity. This attribute could be justified by better contact between Ti species and the zeolitic support as a result of the appropriate loading content. By gradually increasing TiO_2 loading from 10 to 50 wt.%, accumulation of Ti elements in some regions and thus, a decrease in the active sites dispersion can be clearly found which was partly expected regarding the low specific surface area of natural zeolite and high content of loaded titania. The obtained results are also confirmed by surface titanium species density as reported in Table 1. The lower surface titanium density clearly indicates a better dispersion and an increase in the population of the monomeric TiO_2 units as the most active species. According to the Ti dot-mappings, it is obvious that the aluminosilicate surface in the TiO_2 rich composites is seriously covered by the titanium elements which is confirming the surface coverage supposition declared in the FESEM results. This drawback weakens the interaction between the deposited TiO_2 and aluminosilicate and thereupon, leading to the activity loss.

3.1.4. BET analysis

The calculated surface areas for the prepared samples are presented in Table 1. The surface area of bare clinoptilolite and pure TiO_2 are obtained to be 15.73 and 56.23 m^2/g, respectively, in good agreement with values reported in the literature [33,44]. As expected, the specific surface area of raw clinoptilolite is low. As can be seen in Table 1, all the TiO_2-based samples have a larger specific surface area than that of raw zeolite. This can be attributed to the supporting of the high specific surface area of TiO_2 nanoparticles on/in the surface/pores of the natural zeolite. The results clearly show that, increasing the TiO_2 loading over clinoptilolite from 10 to 50 wt.% leads to the rise in the surface area from 22.44 to 34.23 m^2/g. However, high loading of TiO_2 nanoparticles reinforces the possibility of agglomerations formation and zeolite's pores blockage, resulting in a decrease in the photocatalytic performance of these zeolitic composites.

3.1.5. FTIR analysis

FT-IR spectra of the natural aluminosilicate, bare TiO_2, and TiO_2/natural zeolite nanocomposites containing various TiO_2 contents were examined, as shown in Fig. 6. In all the IR spectra, the absorption peaks appeared around 1,400 and 1,640 cm^{-1} wavelengths, are attributed to the hydroxyl bending vibration of interlayer physically adsorbed H_2O

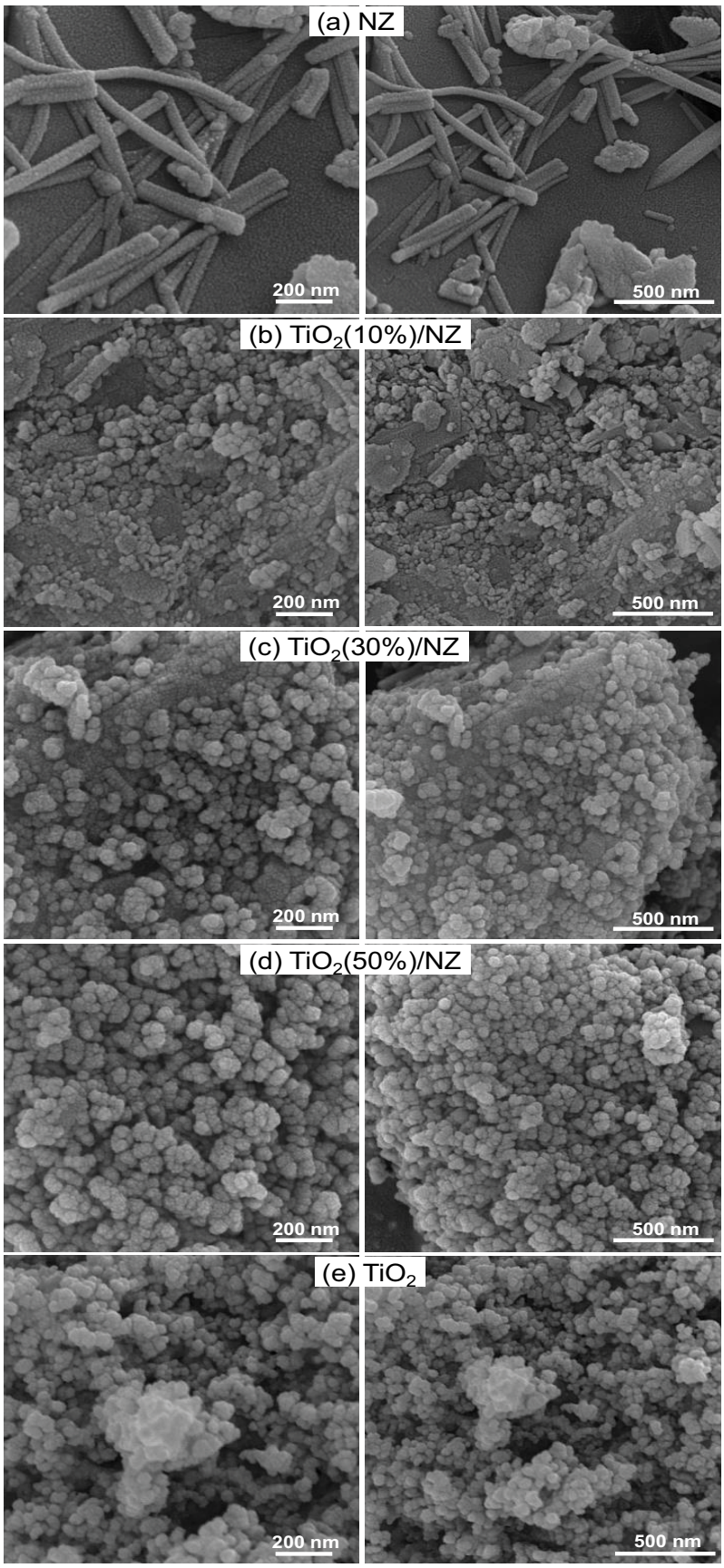

Fig. 4. FESEM images of synthesized photocatalysts: (a) NZ, (b) TiO_2(10%)/NZ, (c) TiO_2(30%)/NZ, (d) TiO_2(50%)/NZ and (e) TiO_2.

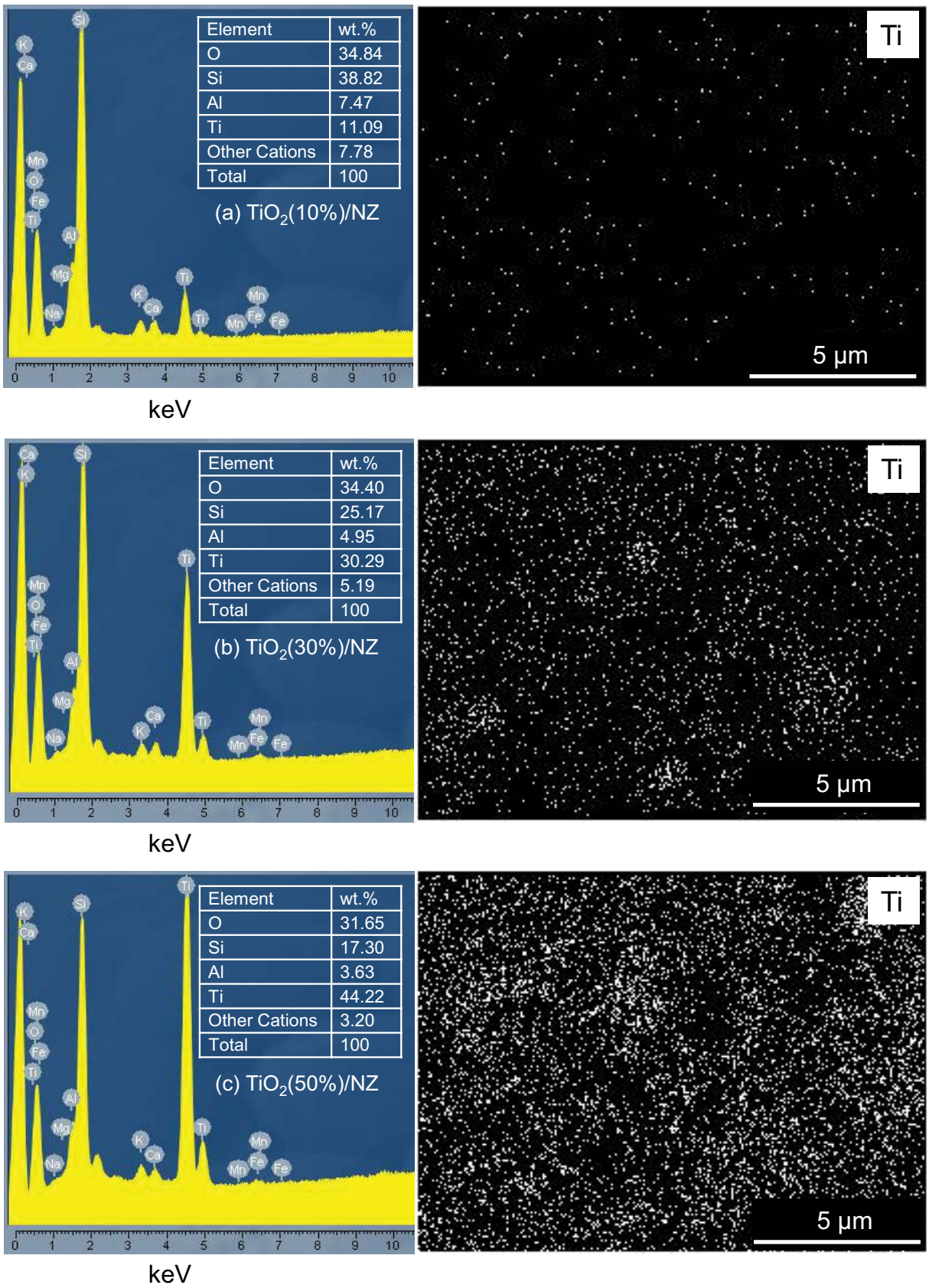

Fig. 5. EDX analysis of synthesized photocatalysts: (a) TiO_2(10%)/NZ, (b) TiO_2(30%)/NZ, and (c) TiO_2(50%)/NZ.

Table 1
Physicochemical properties of TiO_2/natural zeolite photocatalysts

Photocatalyst	Synthesis method	TiO_2 loading (wt.%)	Surface area (m^2/g)	Ti surface density (TiO_2 nm^{-2})	Band gap (eV)
NZ	–	0	56.23	–	–
TiO_2(10%)/NZ	SSD	10	22.44	62.17	3.6
TiO_2(30%)/NZ	SSD	30	25.29	150.68	3.4
TiO_2(50%)/NZ	SSD	50	34.23	162.52	3.3
TiO_2	–	100	15.73	–	3.2

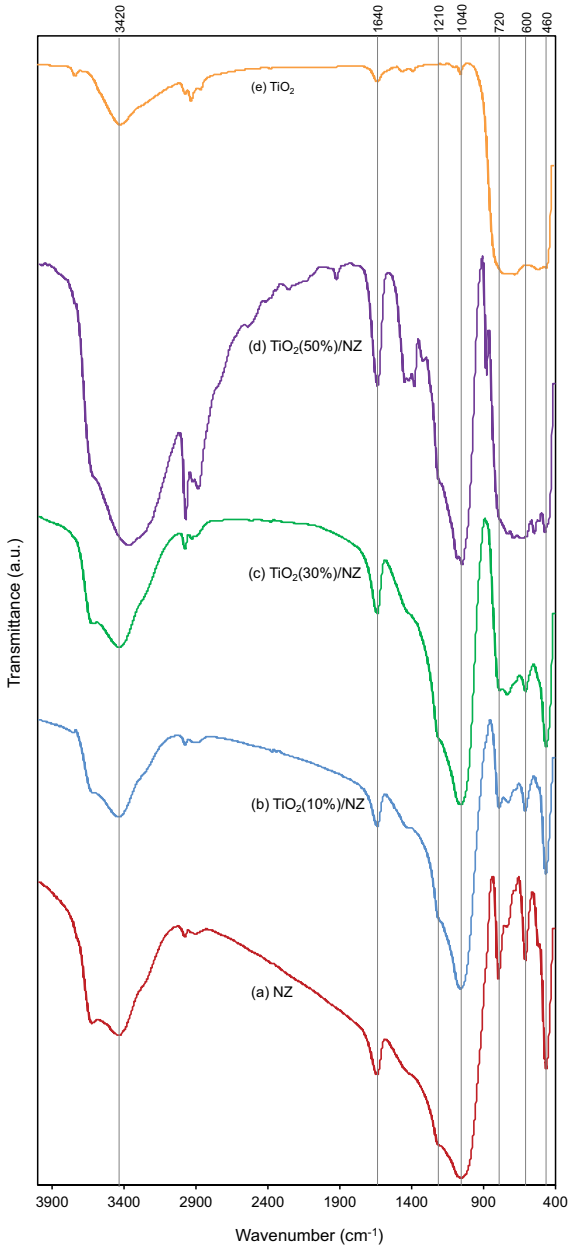

Fig. 6. FTIR spectra of synthesized photocatalysts: (a) NZ, (b) TiO_2(10%)/NZ, (c) TiO_2(30%)/NZ, (d) TiO_2(50%)/NZ and (e) TiO_2.

molecules [45–47]. Moreover, the O–H stretching vibration can also be observed around 3,420 cm^{-1} as a broad peak [48,49]. FTIR spectrum of bare TiO_2 in Fig. 6e displays the broad absorption peak at frequencies below 1,000 cm^{-1} which reflects the stretching vibration of Ti–O–Ti bonds [50,51]. In contrast to the FT-IR spectrum of bare titania, the spectra of TiO_2/natural zeolite photocomposites change obviously. All the clinoptilolite-based materials also represent the characteristic vibration peaks of aluminosilicates. Their spectra are similar to that of bare clinoptilolite. However, a decreasing trend in the intensity of the main zeolitic vibration peaks is observed with the increase in the TiO_2 loading. In detail, the absorption bands detecting around 1,040; 720 cm^{-1}, and ones at 600–460 cm^{-1} attribute to the asymmetrical stretching, the symmetrical stretching, and (O–T–O) deformation, respectively [52–54]. These IR bands are assigned to the internal bonds of the TO_4 (T = Si or Al) tetrahedral structure in the aluminosilicate lattices. The detection of the main zeolitic vibration peaks in the spectra of photocomposites indicates that the aluminosilicate structure remains intact during the preparation process and thereupon, supporting the XRD results. The absence of the IR band around 960 cm^{-1}, which could be attributed to the antisymmetric stretching vibration of the Ti–O–Si bonds, seems to discard the substitution of the tetrahedral Si sites with Ti sites during the synthesis process [23,55]. Therefore, it can be concluded that TiO_2 nanoparticles are deposited on the aluminosilicate structure. This was expected, regarding the SSD method employed in the preparation process.

3.1.6. UV-vis analysis

The diffuse reflectance UV-vis absorption spectra of the synthesized TiO_2/natural zeolite photocatalysts are shown in Fig. 7. No optical absorption was detected for pure clinoptilolite. The absorption edges of the TiO_2/NZ photocatalysts show a blue shift toward a shorter wavelength at about 370 nm compared with P-25 which has a wavelength at about 410 nm. The shifting in the absorption band of titanium oxides to the shorter wavelength can be attributed to the quantization effect due to the decrease of the TiO_2 clusters size and also, the number of agglomerations through dispersing TiO_2 on the surface of the zeolite [56–58]. A slightly greater shift to the lower wavelength in the absorption band can be observed in the TiO_2(10%)/NZ photocatalyst, clearly indicating the better dispersion of the TiO_2 species on its support compared to others. The band gap energy (E_g) of the samples was determined

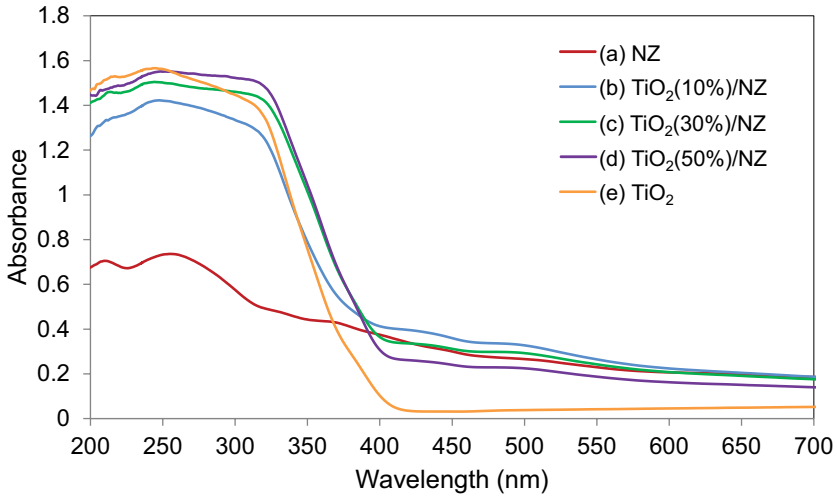

Fig. 7. UV-vis spectra of synthesized photocatalysts: (a) NZ, (b) TiO_2(10%)/NZ, (c) TiO_2(30%)/NZ, (d) TiO_2(50%)/NZ, and (e) TiO_2.

from diffuse reflectance by plotting the square of the Kubelka–Munk function against photon energy based on Tauc theory [1,28]. As can be seen in Table 1, the calculated band gap energies increased from 3.3 to 3.6 eV with decreasing titania loading from 50% to 10% over the TiO_2/natural zeolite photocatalysts. These band gap energies were higher than that of bare TiO_2 (3.2 eV). When TiO_2 was dispersed on clinoptilolite, the band gap was higher (3.6 eV) than that of bare TiO_2, commensurate with decreasing in TiO_2 cluster size and agglomeration numbers as previously reported for supported TiO_2 [57,58]. Thus, DRUVS confirms an appropriate dispersion of titania nanoparticles over clinoptilolite, in good agreement with EDX results.

3.1.7. PL analysis

The photoluminescence (PL) emission spectra have been widely employed to assess the recombination rate of photogenerated electron–hole pairs in semiconductors. Low PL intensity demonstrates a low density of electron–hole recombination, consequently enhancing the separation efficiency of photo-induced electron/hole pairs [59–61]. Fig. 8 displays the PL spectra of bare TiO_2, TiO_2(10%)/NZ, and TiO_2(30%)/NZ excited at 280 nm under similar conditions. As can be seen, all samples exhibit an obvious PL signal centered at ~380 nm. The defects of titania structure and surface oxygen vacancies are responsible for the appearance of these PL signals [62]. As shown in Fig. 8, the signal intensity for the TiO_2/natural zeolite photocomposites was much weaker than that of bare TiO_2. The high intensity of the PL signal observed for bare TiO_2 indicates fast electron–hole pair recombination. However, a considerable PL quenching is observed when TiO_2 is immobilized on the clinoptilolite. This could be related to the electric conductivity of clinoptilolite which can disperse photogenerated electrons in conduction band of the excited semiconductors and reduces the electron–hole recombination. Indeed, the electron-rich zeolite surface can serve as an electron sink and a hole scavenger, facilitating electron transfer from the TiO_2 conduction band to the zeolite surface during the UV irradiation that diminishes the extent of the electron–hole recombination. In addition, the aluminosilicate substrate facilitates the formation of the crystalline anatase phase, restricts the transformation of the crystalline anatase phase to the rutile one, and thereupon, lessens the oxygen vacancy and intrinsic defects of the titanium oxide structure [62]. It is also found that the TiO_2(10%)/NZ photocatalyst shows the lowest PL intensity. This may be because of the uniform dispersion of TiO_2 nanoparticles on the aluminosilicate, will result in the rapid transference of the electrons into the surface in the TiO_2(10%)/NZ sample. The above result reflects that TiO_2(10%)/NZ sample can markedly enhance the separation efficiency of electron–hole pairs and thereupon, a considerable amount of H_2 is produced.

3.2. Photocatalytic performance for hydrogen production

The hydrogen-producing activities for all of the samples in the photocatalytic water splitting under UV irradiation for 4 h are illustrated in Fig. 9. The experiments evidenced no hydrogen evolution over bare clinoptilolite under illumination, indicating that TiO_2 is the only photoactive component of all TiO_2/natural zeolite composites. It is obvious that the presence of clinoptilolite exerts a remarkable impact on the photocatalytic performance of TiO_2. As can be seen, improved photocatalytic activity is achieved for the TiO_2/natural zeolite nanocomposites in comparison with that of pure TiO_2. This can be attributed to the high separation efficiency of electron–hole pairs, better distribution of TiO_2 particles, and lower agglomerations, in accordance with PL, EDX, UV-vis, and FESEM analyses. Among the various TiO_2/natural zeolite nanocomposites, TiO_2(10%)/NZ shows the highest hydrogen production during the photocatalytic reaction. In this case, the H_2 production rate reaches as high as 282.48 μmol/h, which is about four times that of pure TiO_2 (71.16 μmol/h). The different initial photocatalytic activities of the TiO_2-based composites in the water splitting can well be attributed to the difference in their TiO_2 dispersion and recombination rate. In samples with loadings higher than 10%, the agglomerations of TiO_2 particles on the zeolite matrix and the severe coverage of clinoptilolite surface were

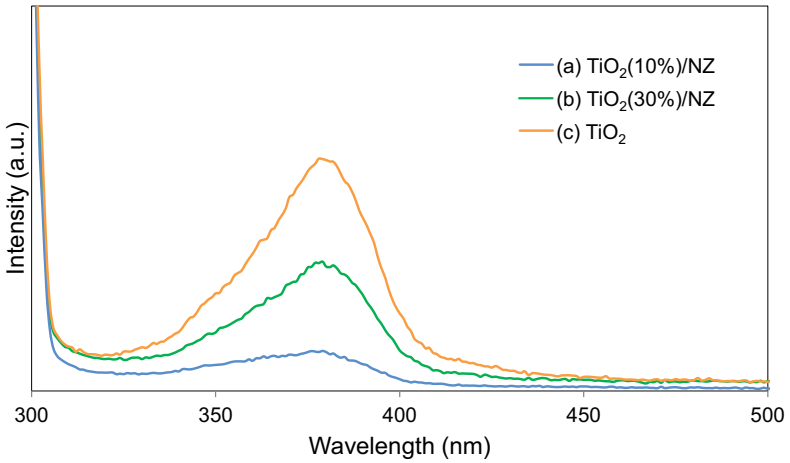

Fig. 8. Photoluminescence spectra of synthesized photocatalysts: (a) TiO_2(10%)/NZ, (b) TiO_2(30%)/NZ, and (c) TiO_2.

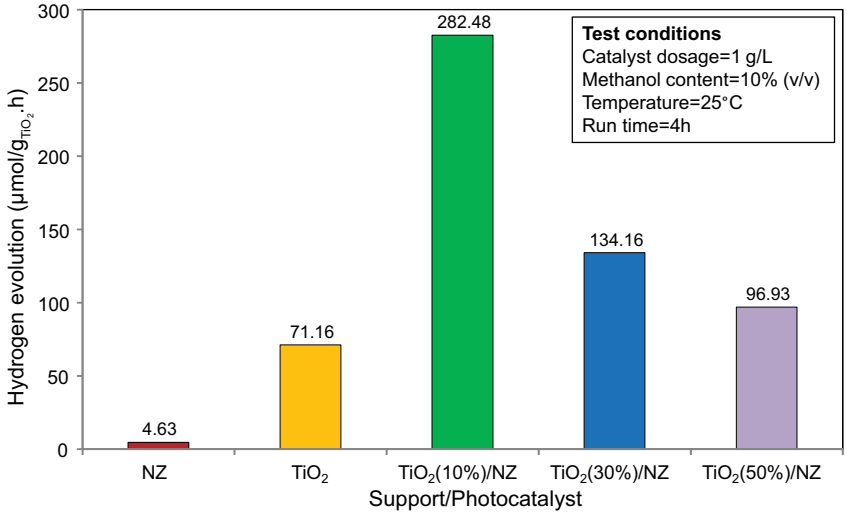

Fig. 9. Hydrogen evolution of synthesized photocatalysts: (a) NZ, (b) TiO_2(10%)/NZ, (c) TiO_2(30%)/NZ, (d) TiO_2(50%)/NZ, and (e) TiO_2.

observed, which weakened the contact between clinoptilolite and TiO_2 and also separation efficiency of electron–hole pairs and hence; resulted in the H_2 production loss.

Fig. 10 shows the time course of hydrogen evolution over the TiO_2(10%)/NZ photocatalyst as the most promising sample. Upon UV-irradiation, H_2 was produced at steadily increasing concentration with the reaction time until it saturated and reached the steady-state plateau. The saturation is due to the establishment of an equilibrium condition, that is, the balance between forward and reverse reaction rates [63].

The reusability of the TiO_2(10%)/NZ nanocomposite was evaluated by performing the recycle experiments under similar conditions and illustrated in Fig. 11. The capability of water splitting was still maintained without a noticeable decrease in the H_2 production after the five-run of photocatalysis test, suggesting the sufficient reusability of TiO_2(10%)/NZ for the hydrogen evolution. It is reasonable to attribute this finding to the presence of clinoptilolite as support, uniform dispersion of TiO_2 nanoparticles, and low number of agglomerations, in accordance with EDX, UV-vis, and FESEM analyses.

In order to better evaluate the synthesized photocatalyst and ensure its performance, the hydrogen production rate was compared with those reported in the literature. Table 2 illustrates different TiO_2-based photocatalysts evaluated in the water-splitting process. According to the activity information and taking into account the process conditions and photocatalysts composition given in Table 2, the photocatalyst of the present study seems to have the appropriate performance towards hydrogen production. It can be seen that the amount of hydrogen production over TiO_2(10 wt.%)/CLT is greater and/or comparable to those of most TiO_2-based photocatalysts. Noticeable activity was found over Pd-TiO_2/ZSM-5 and TiO_2/clinoptilolite photocatalysts. However, TiO_2 in the former catalyst has been promoted by Pd nanoparticles and loaded over ZSM-5 as a synthetic zeolite. Besides, the sonochemical procedure

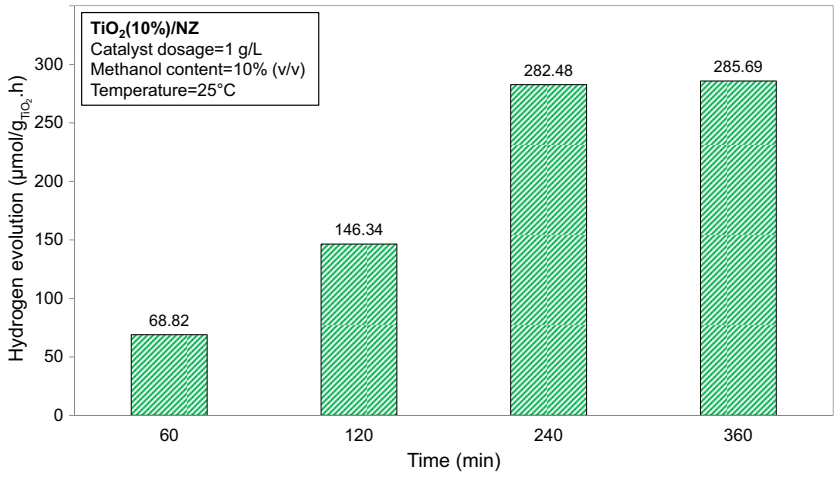

Fig. 10. Time-profiled hydrogen evolution of TiO_2(10%)/NZ photocatalyst.

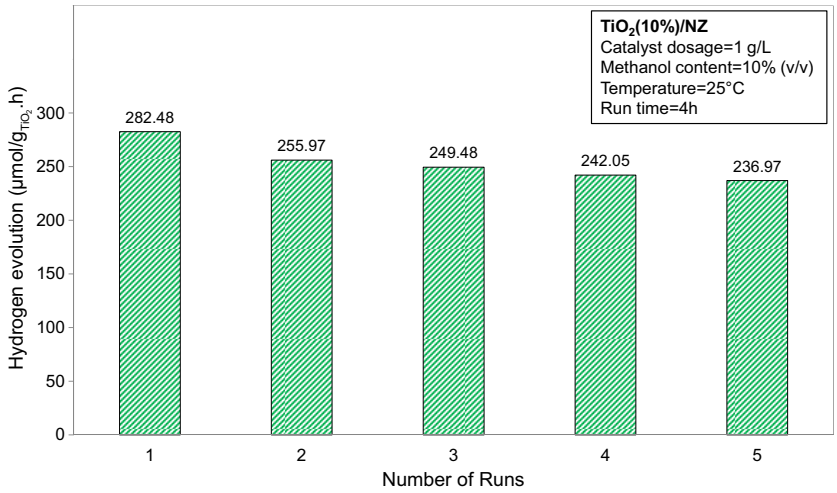

Fig. 11. Reusability of TiO_2(10%)/NZ photocatalyst for hydrogen evolution from water splitting.

Table 2
Photocatalytic performance comparison of different TiO_2-based photocatalysts evaluated for the water splitting process

Photocatalyst	Synthesis method	Irradiation type and time	Photocatalyst dosage (g/L)	Sacrificial agent	H_2 production (μmol g^{-1} h^{-1})	Reference
CuO core/Ag(1 wt.%)-TiO_2	Precipitation	UV-450 W (6 h)	3.33	Methanol	180	[64]
Ag/g-C_3N_4-TiO_2	Hydrothermal	UV-300 W (12 h)	0.5	Triethanolamine	294	[65]
TiO_2/rGO-EDA(1%)	Ultrasound assisted-acylation	UV-LED-12 W	0.625	Ethanol	224.9	[12]
TiO_2/clinoptilolite	Sonochemical	UV-375 W (4 h)	1	Methanol	569.88	[36]
Pd-TiO_2/ZSM-5	Hydrothermal-impregnation	UV	1.5	Methanol	791	[66]
Pt-TiO_2/Clay	Impregnation	UV-500 W	1.5	Methanol	22.3	[67]
Pt-CdS-TiO_2/Zeolite Y	Ion exchange	UV-200 W (8 h)	1.67	Na_2S, Na_2CO_3, NaOH	236	[68]
TiO_2(10 wt.%)/CLT	SSD	UV-375 W (4 h)	1	Methanol	282.48	Present study

has been employed in the letter one. Although the presence of expensive and noble metal promoters, synthetic supports, and also, employing more complex and expensive loading methods can enhance the photocatalytic activity, the photocatalyst cost will also increase significantly and constrain the practical application. Considering the cheap, abundance, and large availability of clinoptilolite and employing low cost and easy solid-state dispersion method, the results obtained in the present work become more important and can be practical.

4. Conclusions

Regarding the results derived, employing low cost, and abundance clinoptilolite as support seems to be a very effective approach to significantly improve the photocatalytic activity of TiO_2 for hydrogen production via the water splitting. The clinoptilolite utilization could not only reduce the recombination of electron–hole pairs but also promote the distribution of metallic particles and decrease the TiO_2 particle agglomerations. The level of the synergetic effect of clinoptilolite utilization strongly depends on TiO_2 loading. These features are more prominent when 10 wt.% of TiO_2 is loaded. However, the promoting effects of clinoptilolite utilization are weakened with the further loading of TiO_2. The excessive loading of TiO_2 (30 and 50 wt.%) severely covered the surface of clinoptilolite, afforded the aggregations of metallic particles, and weakened the contact between clinoptilolite and TiO_2, resulted in a decrease in metallic dispersion and the separation efficiency of electron–hole pairs. The TiO_2(10%)/natural zeolite composite showed the highest photocatalytic activity which alongside sufficient reusability, making it a good choice for photocatalytic water splitting applications.

Acknowledgments

The authors gratefully acknowledge Razi University and University of Kurdistan for the financial support of the project as well as Iran Nanotechnology Initiative Council for complementary financial support.

References

[1] L.S. Yoong, F.K. Chong, B.K. Dutta, Development of copper-doped TiO_2 photocatalyst for hydrogen production under visible light, Energy, 34 (2009) 1652–1661.
[2] M.M. Waskasi, S.M. Hashemianzadeh, O. Mostajabi Sarhangi, A.P. Harzandi, Computational model of hydrogen production by Coumarin-dye-sensitized water splitting to absorb the visible light in a local electric field, Energy Convers. Manage., 62 (2012) 154–164.
[3] D. Gao, W. Liu, Y. Xu, P. Wang, J. Fan, H. Yu, Core-shell Ag@Ni cocatalyst on the TiO_2 photocatalyst: one-step photoinduced deposition and its improved H_2-evolution activity, Appl. Catal., B, 260 (2020) 118190, doi: 10.1016/j.apcatb.2019.118190.
[4] L. Long, J. Li, L. Wu, X. Li, Enhanced photocatalytic performance of platinized CdS/TiO_2 by optimizing calcination temperature of TiO_2 nanotubes, Mater. Sci. Semicond. Process., 26 (2014) 107–111.
[5] S. Boumaza, R. Bouarab, M. Trari, A. Bouguelia, Hydrogen photo-evolution over the spinel $CuCr_2O_4$, Energy Convers. Manage., 50 (2009) 62–68.
[6] N. Dubey, S.S. Rayalu, N.K. Labhsetwar, S. Devotta, Visible light active zeolite-based photocatalysts for hydrogen evolution from water, Int. J. Hydrogen Energy, 33 (2008) 5958–5966.
[7] E. Hong, D. Kim, J.H. Kim, Heterostructured metal sulfide (ZnS–CuS–CdS) photocatalyst for high electron utilization in hydrogen production from solar water splitting, J. Ind. Eng. Chem., 20 (2014) 3869–3874.
[8] S. Obregón, M.J. Muñoz-Batista, M. Fernández-García, A. Kubacka, G. Colón, Cu–TiO_2 systems for the photocatalytic H_2 production: influence of structural and surface support features, Appl. Catal., B, 179 (2015) 468–478.
[9] A. Kudo, Y. Miseki, Heterogeneous photocatalyst materials for water splitting, Chem. Soc. Rev., 38 (2009) 253–278.
[10] J. Shen, R. Wang, Q. Liu, X. Yang, H. Tang, J. Yang, Accelerating photocatalytic hydrogen evolution and pollutant degradation by coupling organic co-catalysts with TiO_2, Chin. J. Catal., 40 (2019) 380–389.
[11] J. Romão, R. Salata, S.-Y. Park, G. Mul, Photocatalytic methanol assisted production of hydrogen with simultaneous degradation of methyl orange, Appl. Catal., A, 518 (2016) 206–212.
[12] H. Li, P. Wang, X. Yi, H. Yu, Edge-selectively amidated graphene for boosting H_2-evolution activity of TiO_2 photocatalyst, Appl. Catal., B, 264 (2020) 118504, doi: 10.1016/j.apcatb.2019.118504.
[13] M. Haghighi, F. Rahmani, F. Kariminejad, R. Akbari Sene, Photodegradation of lignin from pulp and paper mill effluent using TiO_2/PS composite under UV-LED radiation: optimization, toxicity assessment and reusability study, Process Saf. Environ., 122 (2019) 48–57.
[14] M. Ni, M.K.H. Leung, D.Y.C. Leung, K. Sumathy, A review and recent developments in photocatalytic water-splitting using for hydrogen production, Renewable Sustainable Energy Rev., 11 (2007) 401–425.
[15] H. Ahmad, S.K. Kamarudin, L.J. Minggu, M. Kassim, Hydrogen from photo-catalytic water splitting process: a review, Renewable Sustainable Energy Rev., 43 (2015) 599–610.
[16] A. Taheri Najafabadi, F. Taghipour, Physicochemical impact of zeolites as the support for photocatalytic hydrogen production using solar-activated TiO_2-based nanoparticles, Energy Convers. Manage., 82 (2014) 106–113.
[17] A. Chica, Zeolites: promised materials for the sustainable production of hydrogen, ISRN Chem. Eng., 2013 (2013) 1–19, doi: 10.1155/2013/907425.
[18] S. Ikeda, K. Hirao, S. Ishino, M. Matsumura, B. Ohtani, Preparation of platinized strontium titanate covered with hollow silica and its activity for overall water splitting in a novel phase-boundary photocatalytic system, Catal. Today, 117 (2006) 343–349.
[19] Y. Xu, W. Zheng, W. Liu, Enhanced photocatalytic activity of supported TiO_2: dispersing effect of SiO_2, J. Photochem. Photobiol., A., 122 (1999) 57–60.
[20] J.-M. Herrmann, J. Matos, J. Disdier, C. Guillard, J. Laine, S. Malato, J. Blanco, Solar photocatalytic degradation of 4-chlorophenol using the synergistic effect between titania and activated carbon in aqueous suspension, Catal. Today, 54 (1999) 255–265.
[21] S.K. Parayil, H.S. Kibombo, R.T. Koodali, Naphthalene derivatized TiO_2–carbon hybrid materials for efficient photocatalytic splitting of water, Catal. Today, 199 (2013) 8–14.
[22] T. Torimoto, Y. Okawa, N. Takeda, H. Yoneyama, Effect of activated carbon content in TiO_2-loaded activated carbon on photodegradation behaviors of dichloromethane, J. Photochem. Photobiol., A, 103 (1997) 153–157.
[23] S. Gomez, C.L. Marchena, L. Pizzio, L. Pierella, Preparation and characterization of TiO_2/HZSM-11 zeolite for photodegradation of dichlorvos in aqueous solution, J. Hazard. Mater., 258–259 (2013) 19–26.
[24] S. Shen, L. Guo, Hydrothermal synthesis, characterization, and photocatalytic performances of Cr incorporated, and Cr and Ti co-incorporated MCM-41 as visible light photocatalysts for water splitting, Catal. Today, 129 (2007) 414–420.
[25] V. Durgakumari, M. Subrahmanyam, K.V. Subba Rao, A. Ratnamala, M. Noorjahan, K. Tanaka, An easy and efficient use of TiO_2 supported HZSM-5 and TiO_2+HZSM-5 zeolite combinate in the photodegradation of aqueous phenol and p-chlorophenol, Appl. Catal., A, 234 (2002) 155–165.

[26] M. Mahalakshmi, S. Vishnu Priya, B. Arabindoo, M. Palanichamy, V. Murugesan, Photocatalytic degradation of aqueous propoxur solution using TiO_2 and Hβ zeolite-supported TiO_2, J. Hazard. Mater., 161 (2009) 336–343.
[27] N. Dubey, N.K. Labhsetwar, S. Devotta, S.S. Rayalu, Hydrogen evolution by water splitting using novel composite zeolite-based photocatalyst, Catal. Today, 129 (2007) 428–434.
[28] C. Jiang, K.Y. Lee, C.M.A. Parlett, M.K. Bayazit, C.C. Lau, Q. Ruan, S.J.A. Moniz, A.F. Lee, J. Tang, Size-controlled TiO_2 nanoparticles on porous hosts for enhanced photocatalytic hydrogen production, Appl. Catal., A, 521 (2016) 133–139.
[29] C. Wang, H. Shi, Y. Li, Synthesis and characterization of natural zeolite supported Cr-doped TiO_2 photocatalysts, Appl. Surf. Sci., 258 (2012) 4328–4333.
[30] Q. Sun, X. Hu, S. Zheng, Z. Sun, S. Liu, H. Li, Influence of calcination temperature on the structural, adsorption and photocatalytic properties of TiO_2 nanoparticles supported on natural zeolite, Powder Technol., 274 (2015) 88–97.
[31] S. Liu, M. Lim, R. Amal, TiO_2-coated natural zeolite: rapid humic acid adsorption and effective photocatalytic regeneration, Chem. Eng. Sci., 105 (2014) 46–52.
[32] A. Taheri Najafabadi, F. Taghipour, Cobalt precursor role in the photocatalytic activity of the zeolite-supported TiO_2-based photocatalysts under visible light: a promising tool toward zeolite-based core–shell photocatalysis, J. Photochem. Photobiol., A, 248 (2012) 1–7.
[33] F. Rahmani, M. Haghighi, M. Amini, The beneficial utilization of natural zeolite in preparation of Cr/clinoptilolite nano-catalyst used in CO_2-oxidative dehydrogenation of ethane to ethylene, J. Ind. Eng. Chem., 31 (2015) 142–155.
[34] S. Khodadoust, A. Sheini, N. Armand, Photocatalytic degradation of monoethanolamine in wastewater using nano-sized TiO_2 loaded on clinoptilolite, Spectrochim. Acta, Part A, 92 (2012) 91–95.
[35] S. Ko, P.D. Fleming, M. Joyce, P. Ari-Gur, High performance nano-titania photocatalytic paper composite. Part II: preparation and characterization of natural zeolite-based nano-titania composite sheets and study of their photocatalytic activity, Mater. Sci. Eng., B, 164 (2009) 135–139.
[36] R. Akbari Sene, G.R. Moradi, S. Sharifnia, Sono-dispersion of TiO_2 nanoparticles over clinoptilolite used in photocatalytic hydrogen production: effect of ultrasound irradiation during conventional synthesis methods, Ultrason. Sonochem., 37 (2017) 490–501.
[37] R. Akbari Sene, S. Sharifnia, G.R. Moradi, On the impact evaluation of various chemical treatments of support on the photocatalytic properties and hydrogen evolution of sonochemically synthesized TiO_2/clinoptilolite, Int. J. Hydrogen Energy, 43 (2018) 695–707.
[38] F. Rahmani, M. Haghighi, S. Mahboob, CO_2-enhanced dehydrogenation of ethane over sonochemically synthesized Cr/clinoptilolite-ZrO_2 nanocatalyst: effects of ultrasound irradiation and ZrO_2 loading on catalytic activity and stability, Ultrason. Sonochem., 33 (2016) 150–163.
[39] M. Bahrami, A. Nezamzadeh-Ejhieh, Effect of the supported ZnO on clinoptilolite nano-particles in the photodecolorization of semi-real sample bromothymol blue aqueous solution, Mater. Sci. Semicond. Process., 30 (2015) 275–284.
[40] A. Nezamzadeh-Ejhieh, H. Zabihi-Mobarakeh, Heterogeneous photodecolorization of mixture of methylene blue and bromophenol blue using CuO-nano-clinoptilolite, J. Ind. Eng. Chem., 20 (2014) 1421–1431.
[41] Z. Yan, X. Yu, Y. Zhang, H. Jia, Z. Sun, P. Du, Enhanced visible light-driven hydrogen production from water by a noble-metal-free system containing organic dye-sensitized titanium dioxide loaded with nickel hydroxide as the cocatalyst, Appl. Catal., B, 160–161 (2014) 173–178.
[42] T. Sreethawong, C. Junbua, S. Chavadej, Photocatalytic H_2 production from water splitting under visible light irradiation using Eosin Y-sensitized mesoporous-assembled Pt/TiO_2 nanocrystal photocatalyst, J. Power Sources, 190 (2009) 513–524.
[43] M. Park, B.S. Kwak, S.W. Jo, M. Kang, Effective CH_4 production from CO_2 photoreduction using TiO_2/*x* mol% Cu–TiO_2 double-layered films, Energy Convers. Manage., 103 (2015) 431–438.
[44] M.T. Merajin, S. Sharifnia, S.N. Hosseini, N. Yazdanpour, Photocatalytic conversion of greenhouse gases (CO_2 and CH_4) to high value products using TiO_2 nanoparticles supported on stainless steel webnet, J. Taiwan Inst. Chem. Eng., 44 (2013) 239–246.
[45] F. Rahmani, M. Haghighi, Y. Vafaeian, P. Estifaee, Hydrogen production via CO_2 reforming of methane over ZrO_2-doped Ni/ZSM-5 nanostructured catalyst prepared by ultrasound assisted sequential impregnation method, J. Power Sources, 272 (2014) 816–827.
[46] F. Rahmani, M. Haghighi, C_2H_6/CO_2 oxidative dehydrogenation (ODH) reaction on nanostructured CrAPSO-34 catalyst: one-pot hydrothermal vs. conventional hydrothermal/impregnation catalyst synthesis, Korean J. Chem. Eng., 33 (2016) 2555–2566.
[47] A. Nezamzadeh-Ejhieh, S. Khorsandi, Photocatalytic degradation of 4-nitrophenol with ZnO supported nano-clinoptilolite zeolite, J. Ind. Eng. Chem., 20 (2014) 937–946.
[48] F. Rahmani, M. Haghighi, Sono-dispersion of Cr over nano-structured LaAPSO-34 used in CO_2 assisted dehydrogenation of ethane: effects of Si/Al ratio and La incorporation, J. Nat. Gas. Sci. Eng., 27 (2015) 1684–1701.
[49] G. Guo, Y. Hu, S. Jiang, C. Wei, Photocatalytic oxidation of NO_x over TiO_2/HZSM-5 catalysts in the presence of water vapor: effect of hydrophobicity of zeolites, J. Hazard. Mater., 223–224 (2012) 39–45.
[50] H. Li, X. Cui, A hydrothermal route for constructing reduced graphene oxide/TiO_2 nanocomposites: enhanced photocatalytic activity for hydrogen evolution, Int. J. Hydrogen Energy, 39 (2014) 19877–19886.
[51] P.K. Dubey, P. Tripathi, R.S. Tiwari, A.S.K. Sinha, O.N. Srivastava, Synthesis of reduced graphene oxide–TiO_2 nanoparticle composite systems and its application in hydrogen production, Int. J. Hydrogen Energy, 39 (2014) 16282–16292.
[52] H.B. Yener, M. Yılmaz, Ö. Deliismail, S.F. Özkan, Ş.Ş. Helvacı, Clinoptilolite supported rutile TiO_2 composites: synthesis, characterization, and photocatalytic activity on the degradation of terephthalic acid, Sep. Purif. Technol., 173 (2017) 17–26.
[53] H. Zabihi-Mobarakeh, A. Nezamzadeh-Ejhieh, Application of supported TiO_2 onto Iranian clinoptilolite nanoparticles in the photodegradation of mixture of aniline and 2,4-dinitroaniline aqueous solution, J. Ind. Eng. Chem., 26 (2015) 315–321.
[54] A. Nezamzadeh-Ejhieh, N. Moazzeni, Sunlight photo-decolorization of a mixture of Methyl Orange and Bromo-cresol Green by CuS incorporated in a clinoptilolite zeolite as a heterogeneous catalyst, J. Ind. Eng. Chem., 19 (2013) 1433–1442.
[55] W. Zhang, F. Bi, Y. Yu, H. He, Phosphoric acid treating of ZSM-5 zeolite for the enhanced photocatalytic activity of TiO_2/HZSM-5, J. Mol. Catal., A, 372 (2013) 6–12.
[56] M. Anpo, H. Yamashita, Y. Ichihashi, Y. Fujii, M. Honda, Photocatalytic reduction of CO_2 with H_2O on titanium oxides anchored within micropores of zeolites: effects of the structure of the active sites and the addition of pt, J. Phys. Chem. B, 101 (1997) 2632–2636.
[57] A.H. Alwash, A.Z. Abdullah, N. Ismail, Zeolite Y encapsulated with Fe–TiO_2 for ultrasound-assisted degradation of amaranth dye in water, J. Hazard. Mater., 233–234 (2012) 184–193.
[58] H. Yahiro, T. Miyamoto, N. Watanabe, H. Yamaura, Photocatalytic partial oxidation of α-methylstyrene over TiO_2 supported on zeolites, Catal. Today, 120 (2007) 158–162.
[59] J.-D. Lin, S. Yan, Q.-D. Huang, M.-T. Fan, Y.-Z. Yuan, T.T.-Y. Tan, D.-W. Liao, TiO_2 promoted by two different non-noble metal cocatalysts for enhanced photocatalytic H_2 evolution, Appl. Surf. Sci., 309 (2014) 188–193.
[60] T. Sun, E. Liu, J. Fan, X. Hu, F. Wu, W. Hou, Y. Yang, L. Kang, High photocatalytic activity of hydrogen production from water over Fe doped and Ag deposited anatase TiO_2 catalyst synthesized by solvothermal method, Chem. Eng. J., 228 (2013) 896–906.
[61] P. Cheng, Z. Yang, H. Wang, W. Cheng, M. Chen, W. Shangguan, G. Ding, TiO_2–graphene nanocomposites for photocatalytic

hydrogen production from splitting water, Int. J. Hydrogen Energy, 37 (2012) 2224–2230.
[62] C. Wang, Y. Li, Preparation and characterisation of S doped TiO_2/natural zeolite with photocatalytic and adsorption activities, Mater. Technol., 29 (2014) 204–209.
[63] N.-L. Wu, M.-S. Lee, Enhanced TiO_2 photocatalysis by Cu in hydrogen production from aqueous methanol solution, Int. J. Hydrogen Energy, 29 (2004) 1601–1605.
[64] S. Sharma, M.R. Pai, G. Kaur, Divya, V.R. Satsangi, S. Dass, R. Shrivastav, Efficient hydrogen generation on CuO core/$AgTiO_2$ shell nano-hetero-structures by photocatalytic splitting of water, Renewable Energy, 136 (2019) 1202–1216.
[65] X. Wei, C. Shao, X. Li, N. Lu, K. Wang, Z. Zhang, Y. Liu, Facile *in situ* synthesis of plasmonic nanoparticles-decorated g-C_3N_4/TiO_2 heterojunction nanofibers and comparison study of their photosynergistic effects for efficient photocatalytic H_2 evolution, Nanoscale, 8 (2016) 11034–11043.
[66] H. Enzweiler, P.H. Yassue-Cordeiro, M. Schwaab, E. Barbosa-Coutinho, M.H.N. Olsen Scaliante, N.R.C. Fernandes, Evaluation of Pd-TiO_2/ZSM-5 catalysts composition effects on hydrogen production by photocatalytic water splitting, Int. J. Hydrogen Energy, 43 (2018) 6515–6525.
[67] M. Ikeda, Y. Kusumoto, S. Somekawa, P. Ngweniform, B. Ahmmad, Effect of graphite silica on TiO_2 photocatalysis in hydrogen production from water–methanol solution, J. Photochem. Photobiol., A, 184 (2006) 306–312.
[68] J.C. White, P.K. Dutta, Assembly of nanoparticles in zeolite Y for the photocatalytic generation of hydrogen from water, J. Phys. Chem. C, 115 (2011) 2938–2947.